Overview of Toroidal and Poloidal Momentum Transport Studies in JET

T. Tala[1], Y. Andrew[2], K. Crombé[3], P.C. de Vries[2], X. Garbet[4], N. Hawkes[2], H. Nordman[5], K. Rantamäki[1], P. Strand[5], A. Thyagaraja[2], J. Weiland[5], E. Asp[5], Y. Baranov[2], C. Challis[2], G. Corrigan[2], A. Eriksson[5], C. Giroud[2], M.-D. Hua[2], I. Jenkins[2], H.C.M. Knoops[6], X. Litaudon[4], P. Mantica[7], V. Naulin[8], V. Parail[2], K.-D. Zastrow[2] and JET-EFDA contributors[*]

[1]*Association EURATOM-Tekes, VTT, P.O. Box 1000, FIN-02044 VTT, Finland*
[2]*EURATOM/UKAEA Fusion Association, Culham Science Centre, Oxon. OX14 3DB, UK*
[3]*Department of Applied Physics, Ghent University, Belgium*
[4]*Association EURATOM-CEA, CEA/DSM/DRFC Cadarache, St Paul-Lez-Durance, France*
[5]*Association EURATOM-VR, Chalmers University of Technology, Göteborg, Sweden*
[6]*Eindhoven University of Technology, Dept. of Applied Physics, The Netherlands*
[7]*Istituto di Fisica del Plasma CNR-EURATOM, via Cozzi 53, 20125 Milano, Italy*
[8]*Association Euratom-Risø National Laboratory, DK-4000 Roskilde, Denmark*
[*]*See Appendix of M.L. Watkins et al., Fusion Energy 2006 (Proc. 21st Int. Conf. Chengdu 2006), IAEA Vienna (2006)*

Email: tuomas.tala@vtt.fi

Abstract. This paper reports on the recent studies of toroidal and poloidal momentum transport in JET. The ratio of the global energy confinement time to the momentum confinement is found to be close to τ_E/τ_ϕ=1 except for the low density discharges where the ratio is τ_E/τ_ϕ=2–3. On the other hand, local transport analysis of tens of discharges shows that the ratio of the local effective momentum diffusivity to the ion heat diffusivity is χ_ϕ/χ_i≈0.1–0.4 rather than unity, as expected from the global confinement times and used in ITER predictions. The apparent discrepancy in the global and local momentum versus ion heat transport is explained by the fact that momentum confinement within edge pedestal is worse than that of the ion heat and thus, momentum pedestal is weaker than that of ion temperature. Another observation is that while the T_i has a threshold in R/L_{Ti} and profiles are stiff, the gradient in v_ϕ increases with increasing torque and no threshold is found. Predictive transport simulations also confirm that χ_ϕ/χ_i≈0.1–0.4 reproduce the core toroidal velocity profiles well. Concerning poloidal velocities on JET, the experimental measurements show that the carbon poloidal velocity can be an order of magnitude above the neo-classical estimate within the ITB. This significantly affects the calculated radial electric field and therefore, the *E*×*B* flow shear used for example in transport simulations. The Weiland model reproduces the onset, location and strength of the ITB well when the experimental poloidal rotation is used while it does not predict an ITB using the neo-classical poloidal velocity. The most plausible explanation for the generation of the anomalous poloidal velocity is the turbulence driven flow through the Reynold's stress. Both TRB and CUTIE turbulence codes show the existence of an anomalous poloidal velocity, being significantly larger than the neo-classical values. And similarly to experiments, the poloidal velocity profiles peak in the vicinity of the ITB and is caused by flow due to the Reynold's stress.

1. Introduction

It is well known that the *E*×*B* flow shear is one of the major players in quenching turbulence. As the *E*×*B* shear flow is linked to poloidal and toroidal velocities through E_r, understanding of momentum transport is one of the key elements to achieve high fusion performance, good confinement and access to regimes with transport barriers. Through the paper the following definitions in the evaluation of the radial electric field and *E*×*B* shear flow $\omega_{E\times B}$ are used

$$E_r = \frac{1}{eZ_i n_i}\frac{\partial p_i}{\partial r} - v_{\theta,i}B_\phi + v_{\phi,i}B_\theta\,, \qquad \omega_{E\times B} = \frac{r}{q}\frac{\partial\left(qv_E/r\right)}{\partial r} \qquad (1)$$

where Z_i is the charge number, n_i the density, p_i the pressure, $v_{\theta,i}$ the poloidal velocity and $v_{\phi,i}$ the toroidal velocity of the ion species i, v_E is the *E*×*B* velocity, q is the safety factor and B_ϕ and B_θ are toroidal and poloidal components of the magnetic field.

This paper reports on experimental and modelling studies of both toroidal and poloidal momentum transport on JET, investigation of their sources, links to the other transport channels and influences on the radial electric field and Internal Transport Barriers (ITBs).

2. Toroidal Momentum Transport in JET

2.1 Global Momentum and Energy Confinement Times

It has been reported that the toroidal momentum confinement time τ_ϕ is very similar to the energy confinement time τ_E in large tokamaks [1,2,3]. This similarity $\tau_E/\tau_\phi \sim 1$ is further confirmed on JET although at low density ($n_{el} < 15\times10^{19}$m^{-2}) a deviation by a factor of 2–3 is observed as momentum confinement becomes smaller than the energy confinement τ_E/τ_ϕ=2–3, as illustrated in figure 1 [4]. The database consists of a large dataset of more than 1000 pulses from various JET plasma scenarios, such as *L*-mode, ELMy *H*-mode, hybrid and ITBs. τ_E/τ_ϕ and τ_E are defined as the total momentum content divided by the torque and total energy content divided by the total heating power, respectively. The ion energy replacement time τ_i (red dots) is defined as the ion energy content divided by the auxiliary ion heating power (ignoring the ion-electron exchange power). Using the ion energy replacement time instead of the energy confinement time, a very close $\tau_E/\tau_\phi \sim 1$ scaling is also found for low density plasmas.

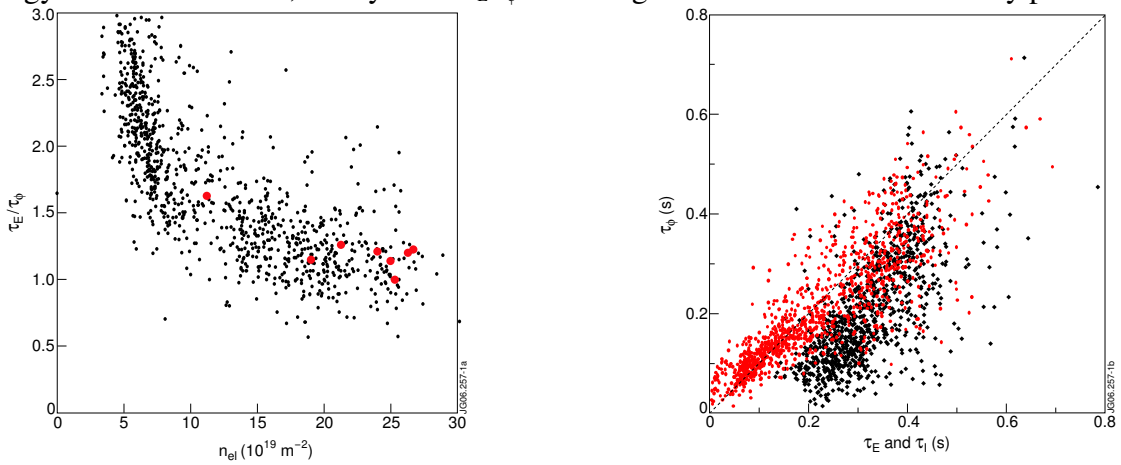

Figure 1. (a) The ratio of energy confinement time to the momentum confinement time as a function of line integrated density over 1000 JET discharges. The red dots will be chosen for detailed local transport analysis, presented in section 2.2. (b) Momentum confinement time as functions of energy confinement time (black dots) and ion replacement time (red dots).

2.2 Local Momentum Transport versus Local Ion Heat Transport

Based on the results from studies of global momentum and energy confinement, one would expect to have equal momentum and ion heat diffusivities in high density plasmas and a momentum diffusivity exceeding that of the ion heat in low density plasmas. However, this will not be the case. The local effective diffusivities are derived from

$$\left.\begin{aligned} S_\phi &= \chi_\phi^{eff}\nabla\Omega \\ Q_i &= n_i\chi_i^{eff}\nabla T_i \end{aligned}\right\} \Rightarrow \qquad P_r = \frac{\chi_\phi^{eff}}{\chi_i^{eff}} = \frac{S_\phi}{Q_i}\frac{n_i T_i}{\Omega}\left(\frac{R/L_{Ti}}{R/L_\Omega}\right) \qquad (2)$$

where Q_i and S_ϕ are the heat and torque fluxes, Ω the angular momentum density, T_i and n_i the ion temperature and density, and L_{Ti} and L_ϕ are local inverse temperature and angular momentum density gradient lengths.

The ratio of the effective momentum diffusivity to the effective ion heat diffusivity, i.e. Prandtl number, can be calculated either using simply equation (2) with scalar quantities from the momentum database or performing interpretive transport simulations with JETTO transport code with self-consistent source power torque densities. This ratio is shown in figure 2 for 9 very high density *H*-mode discharges (red triangles, same as in figure 1), 8 other *H*-

mode pulses with T_i=T_e (black circles) and 25 other *H*-mode pulses with T_i≠T_e (blue circles). The effective diffusivities are averaged over the gradient region between *r*/*a*=0.4 and *r*/*a*=0.7.

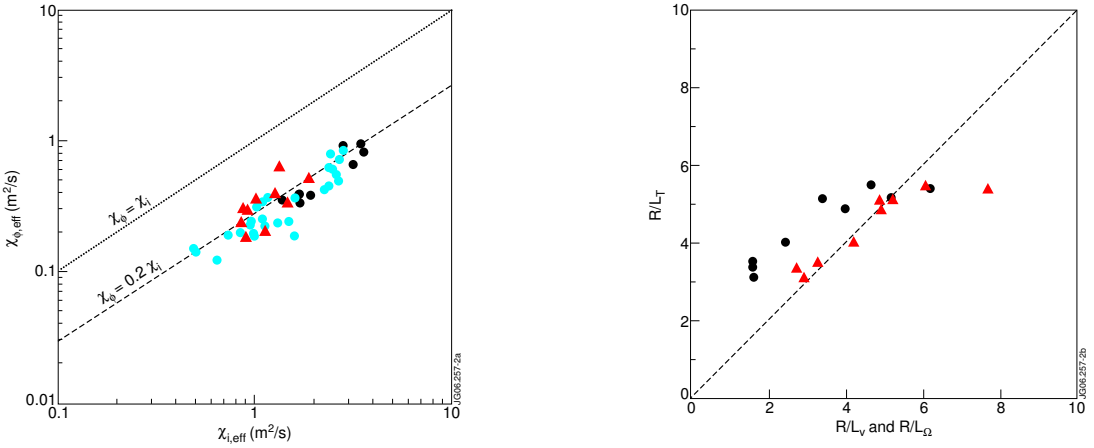

Figure 2. (a) Effective momentum diffusivity versus effective ion heat diffusivity for 9 very high density H-mode discharges (red triangles), 8 H-mode pulses with T_i=T_e (black circles) and 25 H-mode pulses with T_i≠T_e (blue circles). (b) Inverse normalised ion temperature gradient length as a function of inverse normalised momentum density gradient length (red triangles)) and of inverse normalised velocity gradient length (black circles).

It is to note that the ratio χ_ϕ/χ_i=0.1–0.4 for all analysed *H*-mode discharges, and rather independent of the density. In addition, similar ratio χ_ϕ/χ_i=0.1–0.4 is found for *L*-mode and hybrid scenario discharges. This number is smaller than χ_ϕ/χ_i=1, commonly used in ITER predictions and often appearing in the ITG theory [5]. At first sight, there also seems to be an obvious discrepancy between the momentum and ion heat transport with respect to global and local transport properties. Looking into the different terms in equation (2), one can see that ratio of the normalised gradient lengths L_{Ti}/L_Ω is close to or just below one, as illustrated in figure 2(b). However, the ratio of the normalised torque flux to the heat flux $S_\phi/Q_i{\times}T_i n_i/\Omega$ is always below one, around 0.2–0.4 for all discharges in the database. Comparing the ion, electron and torque deposition profiles, it is obvious that the ion heating power is deposited more centrally than the torque and the electron heating power, thus giving rise to the small ratio of $S_\phi/Q_i{\times}T_i n_i/\Omega$. What is not clear yet is firstly, why locally in the gradient region χ_ϕ/χ_i<1 is true while globally τ_E/τ_ϕ≥1 takes place and secondly, why the local ratio of momentum to heat diffusivity is rather independent of the density while the global ratio is not. The database shows that while the core transport is smaller for v_ϕ, the pedestal momentum confinement is worse than that of ion heat and in fact, the edge pedestal is weaker for momentum than for the ion temperature. In addition, as low density discharges tend to have stronger T_i pedestal, the global energy confinement becomes better with decreasing density while the global momentum confinement does not. Another interesting observation in figure 2(b) is that while the normalised inverse ion temperature gradient length has a critical threshold in R/L_{Ti} around 5–6 and T_i profiles become stiff above the threshold, toroidal momentum profiles do not exhibit a threshold in R/L_ϕ, but increasing torque increases R/L_ϕ.

2.3 Transport Simulations of Toroidal Momentum Transport

An extensive transport modelling study has been performed for high and low density ELMy *H*-mode discharges, hybrid scenario discharges and *L*-mode discharges. A new version of the Weiland model that includes self-consistent treatment of the toroidal velocity has been developed [6]. A comparison of the toroidal velocity, ion and electron temperatures and ion heat diffusion coefficients between the experiment and predictions with the new version of the Weiland model as well as with GLF23 transport model is illustrated in figure 3. The main dif-

ference between the two high density ELMy *H*-mode discharges with equal T_i and T_e is that pulse 57984 is expected to be clearly above the critical ion temperature gradient for ITG to be unstable (left frames) while pulse 60870 (right frames) is below the ITG threshold. The stability is calculated with the linear gyrokinetic flux tube code KINEZERO [7]. For the ITG unstable discharge, both models reproduce the experimental temperatures very well, and GLF23 also predicts v_ϕ extremely well whereas the Weiland model tends to underestimate the central v_ϕ. Including the momentum pinch will increase central v_ϕ, but leads often to numerical problems and thus will not be considered here. This kind of good agreement (better in most cases) between the predictions and experiment is generally true for other discharges existing in the database that are clearly above the ITG threshold. On the other hand, for the discharge that KINEZERO finds ITG stable, both the Weiland model and GLF23 overpredict the temperatures significantly. In fact, there are several high density ELMy *H*-mode discharges that KINEZERO finds stable, and Weiland model and GLF23 massively overpredict temperatures and v_ϕ. Thus, experimentally something must drive transport above neo-classical level and prevent the T_i, T_e and v_ϕ profiles from rising up to their predicted levels. Both models also predict that the ratio of χ_ϕ/χ_i is around 0.2–0.4 in the gradient region except for those shots with no unstable modes. Then the ratio is exactly one as we have assumed that the neo-classical momentum diffusivity is equal to the neo-classical ion heat diffusivity in all the simulations.

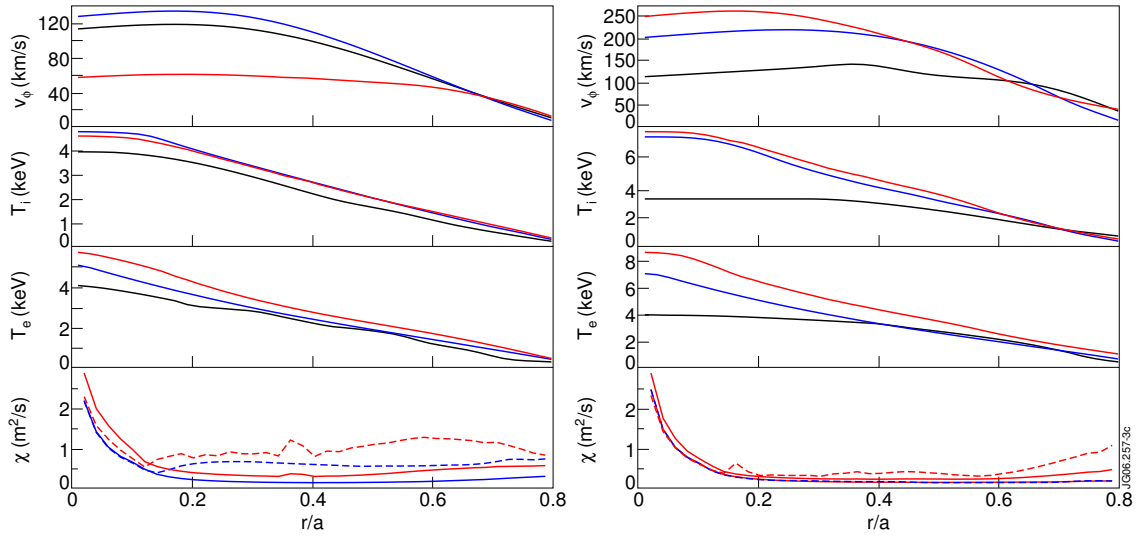

Figure 3. (a) Experimental (black curves) and predicted by GLF23 (blue curves) and Weiland model (red curves) of v_ϕ (upper frame), T_i (second frame) and T_e (third frame) for pulse no. 57894. Fourth frame shows χ_ϕ and χ_i predicted by the GLF23 (blue dashed and blue) and by the Weiland (red dashed and red), respectively. (b) As for (a), but for JET pulse no. 60870.

3 Poloidal Rotation in JET ITB Plasmas

3.1 Experimental Results

The experimental ion temperature, density and toroidal and poloidal velocities are shown in figure 4 for a typical JET ITB discharge at four instants. The poloidal velocities can reach values of up to v_θ=-50km/s within the fully developed ITB while before ITB formation they stay around 5km/s. A negative value of v_θ is in the ion diamagnetic drift direction. The comparison between carbon poloidal velocity v_θ and the neoclassical predictions for the carbon ion velocity calculated with the neo-classical transport code NCLASS [8] is shown in figure 5 (left frames) for two JET discharges. The measured carbon v_θ is an order of magnitude larger within the ITB than its neo-classical estimate for both cases. Even the sign of the measured

carbon v_θ is different from the neo-classical one in some radial regions, and furthermore, can change sign within the ITB. Similar results are obtained for other JET ITB discharges [9]. Due to the large difference in v_θ between the measured value and the neo-classical estimate, the evaluated radial electric field E_r (from equation (1)) depends on the source of v_θ and is in most cases much larger when the measured v_θ is used instead of the neo-classical one, as shown in figure 5 (right frames).

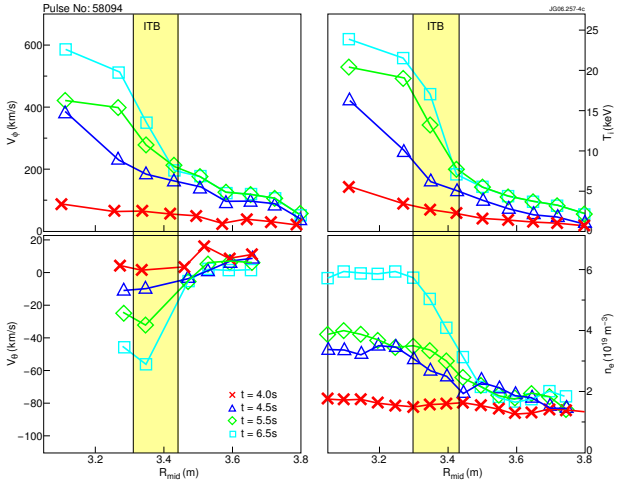

Figure 4. Toroidal and poloidal rotation, ion temperature and electron density profiles at four instants for a typical JET ITB discharge. The yellow shaded region indicates the location of the ITB.

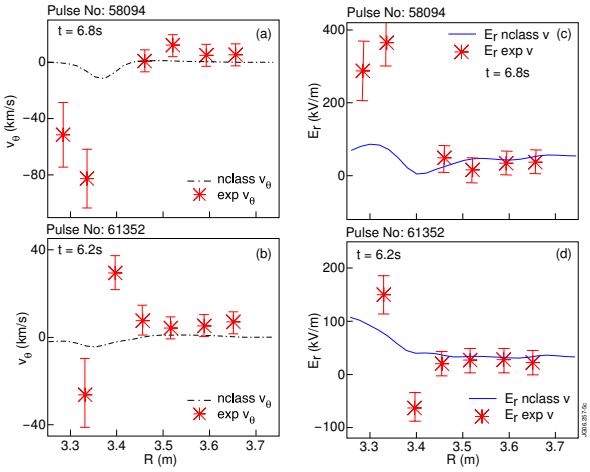

Figure 5. (a) and (b) Comparison of measured carbon v_θ profiles with neoclassical predictions by NCLASS. (c) and (d) E_r profiles calculated using the force balance equation, with the measured (stars) and the NCLASS v_θ (line)

3.2 Predictive Transport Modelling Using the Measured Poloidal Velocities

Predicting the dynamics and physics of the ITBs has turned out to be one of the biggest challenges for transport models. In particular the first-principle transport models often fail to predict the onset of the ITB or the radial location correctly [10]. There are most probably several reasons for having difficulties in reproducing ITBs, but one of the reasons, not taken into account earlier is that past transport simulations have assumed that the poloidal rotation velocity is neo-classical. As shown earlier, this is not a good assumption and therefore, the used *E*×*B* flow shear will not be appropriate.

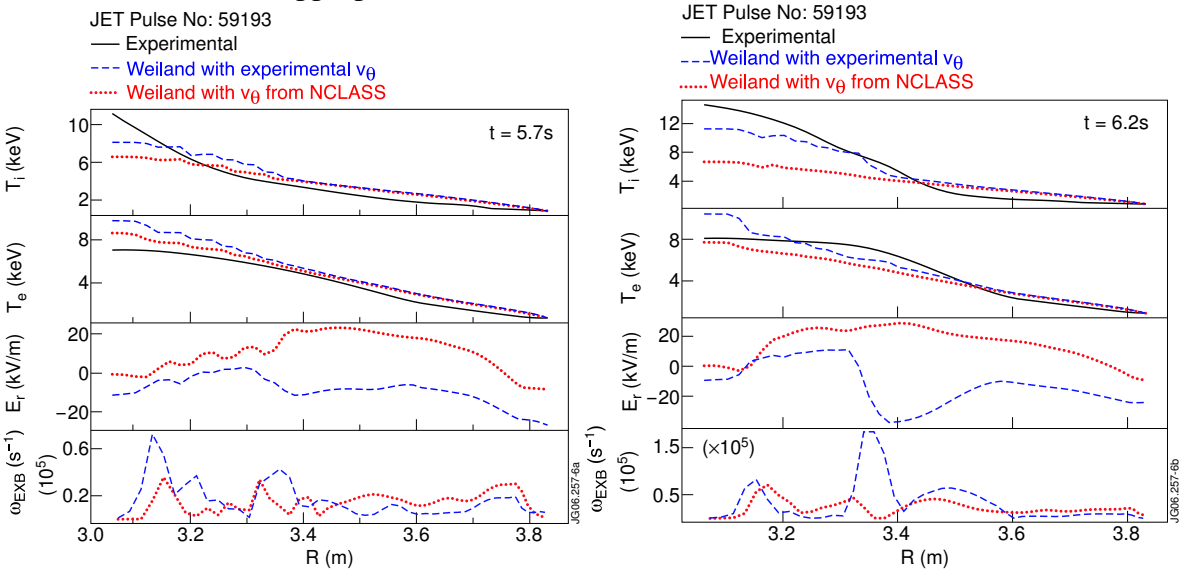

Figure 6. Predictions for the ion and electron temperatures, radial electric field and $\omega_{E\times B}$ shearing rate before the ion ITB formation (left frame) and after it (right frame).

In order to illustrate the changes in the modelling results due to the different source of v_θ, two predictive simulations with the Weiland transport model are compared in figure 6 [11]. The only difference between the two simulations is that the first one (red curves) uses the neo-classical poloidal velocity from NCLASS whereas the second one (blue curves) employs the experimentally measured v_θ in the calculation of E_r and ω_{ExB} flow shearing rate.

In the case when the experimental poloidal rotation is used, the Weiland model predicts the ion ITB just at the right radial location and right instant with roughly the same ITB strength as measured in the experiments. On the other hand, otherwise an identical simulation except with v_θ from NCLASS does not exhibit any sign of an ITB and the agreement in T_i and T_e is much worse. Worth noting are also the large differences in E_r and ω_{ExB} shearing rates.

3.3 Turbulence Simulations of the Generation of the Poloidal Rotation Velocity

As shown earlier, the measured poloidal velocity is certainly not neo-classical and indeed, significantly affects the predictions of the transport simulations. However, the cause for the difference between measured and neo-classical v_θ, i.e. the source of the anomalous poloidal velocity, is not fully clear at present. Generation of the poloidal flow has been studied with the TRB turbulence code [12] solving fluid equations for ITG/TEM turbulence and with non-linear 3D global electromagnetic fluid turbulence code CUTIE [13]. The time evolution of the deuterium poloidal velocity v_θ in those turbulence codes can be written as in equation (3) (ignoring the NBI source term)

$$\frac{\partial\langle v_\theta\rangle}{\partial t} = -\upsilon_{NC}\left(\langle v_\theta\rangle - \langle u_{NC}\rangle\right) - \frac{\partial}{r^2\partial r}\left\langle r^2\tilde{v}_{E,\theta}\tilde{v}_{E,r}\right\rangle + \frac{\left\langle \tilde{j}\tilde{B}\right\rangle}{m_i n_i} + \frac{\langle S_{NBI,\theta}\rangle}{m_i n_i}, \tag{3}$$

where ν_{NC} represents the neo-classical viscous damping term, u_{NC} is the neo-classical poloidal rotation velocity, $\Pi_{RS}=\langle v_{E,\theta}v_{E,r}\rangle$ is the Reynolds stress, $\left\langle \tilde{j}\tilde{B}\right\rangle/m_i n$ the Maxwells stress and $S_{NBI,\theta}$ represents the source (torque) from the NBI in the poloidal direction. However, the experiments show no evidence on any clear correlation between the changes in v_θ after changes in the NBI power, indicating that the last term is small and thus will not be considered later.

The poloidal velocity v_θ is supposed to be damped to the neo-classical level u_{NC} because of the large neo-classical viscous damping term ν_{NC}, proportional to ion-ion collisions. The orbit squeezing effect due to large temperature and density gradient may, however violate the neo-classical theory and thus could decrease ν_{NC}. On the other hand, the orbit squeezing effect is not expected to be large enough to explain the difference of an order of magnitude between the measured and neo-classical carbon poloidal velocity.

Consequently, the main candidate to explain the anomalous v_θ is thought to be the turbulence driven poloidal velocity through the Reynold's and Maxwell's stresses. For standard ITG turbulence, the quasi-linear expression of the Reynolds stress can be written as

$$\Pi_{RS,QL} = \mu\partial_r V_E \quad ; \quad \mu = 2\frac{T_D}{T_e}\frac{q}{\left|\bar{k}_\theta s\rho_D\right|}\frac{L_p}{v_{TD}}\left\langle\left|\tilde{v}_E\right|^2\right\rangle \tag{4}$$

where $V_E=-E_r/B$ is the $E\times B$ drift poloidal velocity, $\bar{k}_\theta$ is an average poloidal wavenumber, ρ_D and v_{TD} are the deuterium Larmor radius and thermal velocity, L_p the pressure gradient length, and s is the magnetic shear. The relationship between V_E and v_θ is given by the force balance equation (1). Solving equation (3) in steady-state, one can see that the influence of turbulence appears as a negative-viscosity effect when the 2nd order differential equation is solved for V_E.

Simulations with the TRB code of a plasma with ρ_*=0.01 (standard *H*-mode plasma with no ITB) indicate a shift of the deuterium velocity in the electron diamagnetic direction of a fraction of the diamagnetic velocity, as shown on figure 7. As the deuterium poloidal velocity $v_{\theta,D}$ is almost half of its diamagnetic velocity, the carbon poloidal rotation $v_{\theta,C}$ is, according to force balance equation, significantly higher than the carbon neo-classical velocity. Consequently, it seems very plausible that the source of the measured anomalous v_θ is driven by the turbulence through the Reynold's stress.

TRB simulations have also been performed with a reversed *q*-profile, leading to the onset of an ITB. Again, a large non-neoclassical poloidal velocity is observed, which is maximum inside the barrier, qualitatively in accordance with experimental results. This is shown in figure 8. However, it is directed in the electron diamagnetic direction, whereas for most of the JET ITB discharges v_θ is observed to be in the ion diamagnetic direction within the ITB. On the other hand, there are also discharges where the measured poloidal rotation is shifted in electron diamagnetic direction, such as pulse no. 61352 in figure 5.

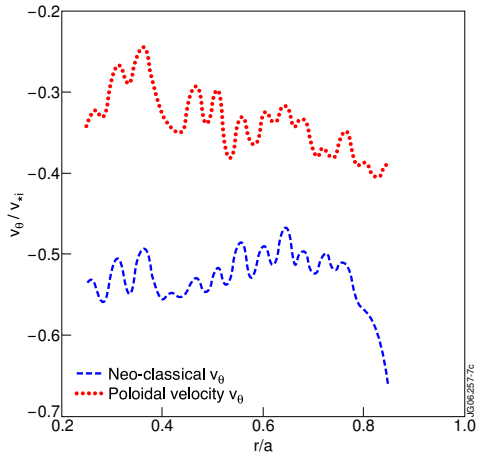

Figure 7. Radial profiles of predicted $v_{\theta,D}$ and neoclassical deuterium velocity calculated by the TRB code. The velocity unit is a diamagnetic velocity in units T/eBa and positive values are in the electron diamagnetic direction.

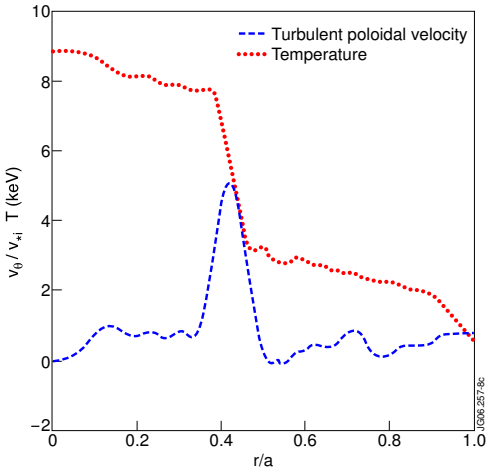

Figure 8. Radial profiles of ion temperature and the turbulent poloidal velocity (v_θ - u_{NC}) due to turbulence calculated with the TRB code for a case with a reversed q-profile. Units as in figure 7.

Similar kinds of simulations to study the turbulence generation of poloidal velocity have been performed with non-linear 3D global electromagnetic fluid turbulence code CUTIE. The simulations are carried out using the input data from pulse 58094 (shown in figure 4) at *t*=5.5s. The predicted ion temperature and poloidal velocity are compared with experimental ones in figure 9. CUTIE predicts a significant peak in v_θ, much higher than the neo-classical v_θ, in the inner side of the ITB flowing in the ion diamagnetic direction. The predicted time averaged v_θ is qualitatively similar to the experimental values, although it exhibits large fluctuations in the whole core region. According to CUTIE, the electrostatic part, i.e. force due to the Reynold's stress plays the dominant role in generating v_θ for this shot, but in some other cases the Maxwell's stress can be of the same order. It is difficult to determine the forces precisely because they depend on the time interval over which they are averaged. Although Reynold's stress appears clearly as the dominant one, it is not conclusive. Both codes neglect the possible role of geodesic acoustic modes in flow generation.

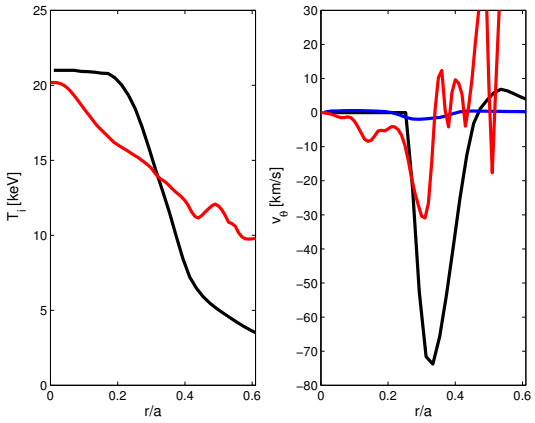

Figure 9. Comparison of T_i and v_θ between the CUTIE simulation (red), experiment (black) and neo-classical v_θ (blue) for JET discharge 58094 at t=5.5s.

4. Summary

The toroidal momentum database confirmed the earlier observation that τ_E/τ_ϕ~1 although at low density, τ_E becomes larger by a factor of 2–3. On the other hand, locally in the gradient region a ratio of χ_ϕ/χ_i=0.1–0.4 is determined. While the core momentum transport is smaller that of the ion heat, the edge momentum transport is larger, thus explaining the discrepancy between the global and local momentum versus ion heat transport. To extrapolate the toroidal velocities in the ITER core plasma, a reassessment is needed as the standard assumption χ_ϕ/χ_i=1 is not justified from the JET results. The self-consistent transport simulations of toroidal momentum with the Weiland model and GLF23 predict v_ϕ roughly with the same accuracy as T_i. The possible role of an inward momentum pinch and a more thorough analysis of the edge momentum transport are the major elements to be assessed in future.

Anomalous carbon poloidal velocities, exceeding the neo-classical estimate by a factor of 10, are measured within the ITB on JET. This changes the calculated E_r and ω_{ExB} shearing rates significantly, and improves the success of first-principle transport models to predict the dynamics of the ITBs. Turbulence simulations show the generation of the anomalous poloidal velocity in the vicinity of the ITB due to poloidal force through the Reynold's stress, qualitatively in agreement with the experimental observations. Major unresolved issues are the causality of anomalous v_θ and the onset of the ITB and the sign of v_θ, as neither the experiments nor the simulations reveal any clear parametric dependence.

[1] Zastrow K.-D. *et al.* 1998 *Nucl. Fusion* **38** 257.
[2] Kallenbach A. *et al.* 1991 *Nucl. Fusion* **33** 595.
[3] de Grassie J.S. *et al.* 2003 *Nucl. Fusion* **43** 142.
[4] de Vries P.C. *et al.* 2006 « Plasma Rotation amd Momentum Transport Studies at JET» *accepted for publication in Plasma Phys. Control. Fusion.*
[5] Mattor N and Diamond P. 1988 *Phys. Fluids* **31** 1180.
[6] Weiland J. and Nordman H. 2006 *Proc. 33rd European Physical Society Conf. on Control. Fusion and Plasma Phys. (Rome, Italy, 19 – 23 June 2006) ECA* **30** P2.186.
[7] Bourdelle C *et al.* 2002 *Nucl. Fusion* **42** 822.
[8] Houlberg W. *et al.* 1997 Phys. Plasmas **4** 3231.
[9] Crombé K. *et al*. 2005 *Phys. Rev. Lett*. **95** 155003
[10] Tala T. *et al.* 2006 *Nucl. Fusion* **46** 548.
[11] Tala T. *et al.* 2005 *Proc. 32nd European Physical Society Conf. on Controlled Fusion and Plasma Physics (Tarragona, Spain, 27 June – 1 July 2005) ECA* **29** P4.044.
[12] Garbet X. and Waltz R.E. 1996 *Phys. Plasmas* **3**1898.
[13] Thyagaraja A. 2000 *Plasma Phys. Control. Fusion* **42** B255.